

University of Groningen

Direct Irradiation of Phenol and Para-Substituted Phenols with a Laser Pulse (266 nm) in Homogeneous and Micro-heterogeneous Media. A Time-Resolved Spectroscopy Study

Siano, Gastón; Crespi, Stefano; Bonesi, Sergio M.

Published in:
Journal of Organic Chemistry

DOI:
[10.1021/acs.joc.0c02031](https://doi.org/10.1021/acs.joc.0c02031)

IMPORTANT NOTE: You are advised to consult the publisher's version (publisher's PDF) if you wish to cite from it. Please check the document version below.

Document Version
Publisher's PDF, also known as Version of record

Publication date:
2020

[Link to publication in University of Groningen/UMCG research database](#)

Citation for published version (APA):

Siano, G., Crespi, S., & Bonesi, S. M. (2020). Direct Irradiation of Phenol and Para-Substituted Phenols with a Laser Pulse (266 nm) in Homogeneous and Micro-heterogeneous Media. A Time-Resolved Spectroscopy Study. *Journal of Organic Chemistry*, 85(21), 14012-14025.
<https://doi.org/10.1021/acs.joc.0c02031>

Copyright

Other than for strictly personal use, it is not permitted to download or to forward/distribute the text or part of it without the consent of the author(s) and/or copyright holder(s), unless the work is under an open content license (like Creative Commons).

The publication may also be distributed here under the terms of Article 25fa of the Dutch Copyright Act, indicated by the "Taverne" license. More information can be found on the University of Groningen website: <https://www.rug.nl/library/open-access/self-archiving-pure/taverne-amendment>.

Take-down policy

If you believe that this document breaches copyright please contact us providing details, and we will remove access to the work immediately and investigate your claim.

Downloaded from the University of Groningen/UMCG research database (Pure): <http://www.rug.nl/research/portal>. For technical reasons the number of authors shown on this cover page is limited to 10 maximum.

Phenol radical-cations have been observed directly in matrices at low temperature,¹² strong acids,^{11b} and gas-phase clusters.¹³ Evidence of their existence has been provided by CINDP and ESR spectroscopies.¹⁴ Several phenol radical-cations have been characterized with both pulse radiolysis and laser flash photolysis spectroscopies in acetonitrile and *n*-butyl chloride at room temperature.^{9b,10i,h,15} Oxidation of phenols by pulse radiolysis in the presence of persulfate or azide anions in acetonitrile has demonstrated the formation of radicals and radical-cations, and in the last case, under basic conditions, excitation of the corresponding phenolates provided the phenoxyl radicals.¹⁶

Direct irradiation (308 nm) of α -tocopherol in micellar solutions of HTAC and SDS have shown the formation of the α -tocopheroxyl radical and this transient was found to be relatively long-lived in micellar solutions allowing the slow reaction with glutathione.^{17a} In addition, the same radical transient has been detected in micellar media using time-resolved Raman and laser flash photolysis spectroscopies.^{17b} Recently, α -tocopheroxyl radical has been formed by reaction of the corresponding phenol with photochemically generated *tert*-butoxyl radical in SDS solution and has been detected by laser flash photolysis and EPR measurements. The transient decay was prolonged, showing a rate constant of $75 \text{ M}^{-1} \text{ s}^{-1}$. However, in the presence of several green tea polyphenols, the rate constants increased significantly, regenerating the α -tocopherol.^{17c}

Resveratrol is another phenol that has been studied by laser flash photolysis technique in micellar solution using SDS, DTCA, and TX-100 as surfactants. In these studies, the resveratroxyl radical was generated efficiently under direct irradiation with a laser pulse of 266 nm.¹⁸ Formation of this transient has also been observed when direct irradiation of resveratrol in aqueous cyclodextrin solution was carried out with 355 nm light and, in the presence of ascorbate, regeneration of the phenol occurred efficiently.¹⁹ In this particular example, the resveratroxyl radical was formed within the hydrophobic core of the cyclodextrin.

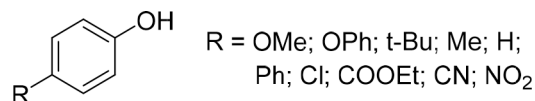
Recently, the photophysical and photochemical properties of resveratrol have been investigated in water and acetonitrile under direct irradiation with a laser pulse of 266 or 355 nm. Both the key transient species, *viz.* phenoxyl radical and phenol radical-cation, were observed.²⁰ The photoreaction involves the singlet excited state and is a two-photon ionization process. In acetonitrile the transient radical-cation deprotonates with a rate constant of $2.7 \times 10^5 \text{ s}^{-1}$ yielding the long-lived phenoxyl radical. Water (0.75%) stabilized the intermediate that decayed with rate constant around $1 \times 10^8 \text{ M}^{-1} \text{ s}^{-1}$.

On the other hand, the photochemical process of 8-hydroxy-1,3,6-pyrenetrisulfonic acid (PyOH) involves the photoelectron ejection from PyO^- to produce PyO^\bullet and $\text{PyO}^{\bullet-}$ under visible laser excitation (470 nm).²¹ The kinetic rate constants for phenolic antioxidants with PyO^\bullet were mostly reliant on the ionic strength depending on the antioxidant phenolate/phenol dissociation constant. Also, the study carried out in Triton-X100 micellar solution showed that the apparent rate constants depend on the partition of the phenolic antioxidants between the micelles and the aqueous media. The observed rate constants varied between 1.41×10^6 and $6.22 \times 10^6 \text{ M}^{-1} \text{ s}^{-1}$.

The above results show that there is considerable interest in the photochemistry of phenol derivatives, but to our knowledge, a systematic photochemical study on a series of *para*-substituted phenols has not been performed yet. Therefore, fostered by our results on the photo-Fries reaction, in this work we describe the

results obtained from a systematic laser flash photolysis investigation (laser pulse of 266 nm) of a series of *para*-substituted phenols (see Chart 1) in homogeneous (cyclo-

Chart 1. Structures of the Phenol Derivatives



hexane, acetonitrile, and methanol) and heterogeneous (SDS micellar solution) media at room temperature and under nitrogen atmosphere. Such a study should contribute to knowledge about the stability, reactivity, and chemical consequences of the transient species *viz.* phenol radical-cations and phenoxyl radicals. Furthermore, the phenol radical-cations are expected to behave like acid compounds, and the acidity of such a transient can be tuned depending on the electronic properties of the substituents. In fact, it is expected that phenol radical-cations bearing electron-withdrawing substituents would increase the acidity of the radical-cation transients generating more readily the corresponding phenoxyl radicals. This behavior will be demonstrated by applying the Hammett linear correlation and the Brønsted plots.

RESULTS

Irradiation of *Para*-Substituted Phenols in Homogeneous Media with a Laser Pulse. Direct irradiation of a series of *para*-substituted phenols (see Chart 1) in different solvents (cyclohexane, acetonitrile and methanol) was carried out with a 266 nm laser pulse under nitrogen atmosphere. The experiments showed the formation of two transient species *viz.* the phenol radical-cation and the phenoxyl radical. Both species have distinct lifetimes: the phenol radical-cations show short lifetime (lower than $10 \mu\text{s}$) while the phenoxyl radicals are species with lifetimes higher than $20 \mu\text{s}$. Moreover, the transient radical-cation showed a broad absorption band located between 390 and 490 nm while the phenoxyl radical showed two characteristic bands centered at 320 nm and 400–410 nm (see Scheme 1) which are similar to those reported in the literature.^{9,15}

Representative transient absorption spectra of some *para*-substituted phenols in acetonitrile under nitrogen atmosphere recorded after the laser pulse of 266 nm are shown in Figure 1. All the transient absorption spectra recorded in cyclohexane, acetonitrile and methanol in the same experimental conditions are collected in Figure S1 (see Supporting Information).

In order to establish whether the transient absorption spectra is the overlapping of absorption spectra of the phenoxyl radical and phenol radical-cation, respectively, we have performed additional experiments. *p*-Phenoxyphenol was selected as a probe because the absorption of both transients are partially overlapped.^{9–11} Hence, we have irradiated a solution of *p*-phenoxyphenol in an acetonitrile water (9:1) mixture in the presence of sodium persulfate with a laser pulse of 266 nm under nitrogen atmosphere (see Scheme 2). This methodology affords the selective formation of radical-cations in solution, as reported in the literature.^{16a}

Thus, we have recorded the transient absorption spectra of *p*-phenoxyphenol in acetonitrile in the absence (black solid line) and the presence of $\text{K}_2\text{S}_2\text{O}_8$ (blue solid line) under nitrogen atmosphere with a laser pulse of 266 nm which are shown in Figure 2a. In the same figure, the differential spectrum (red solid line) shows the estimated absorption spectra of the *p*-

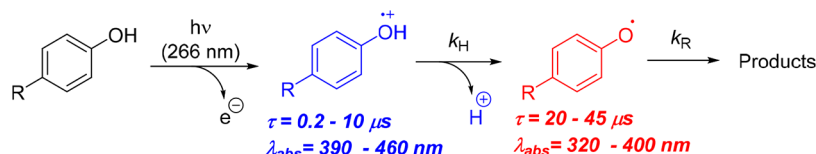
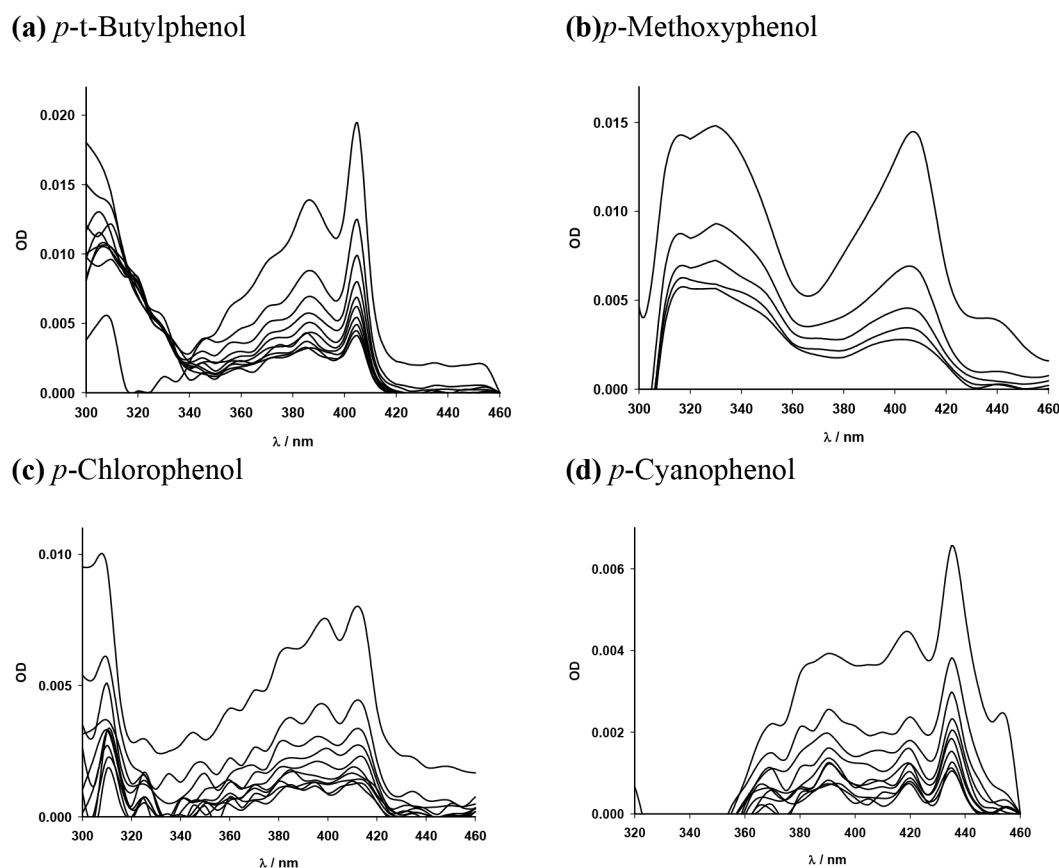
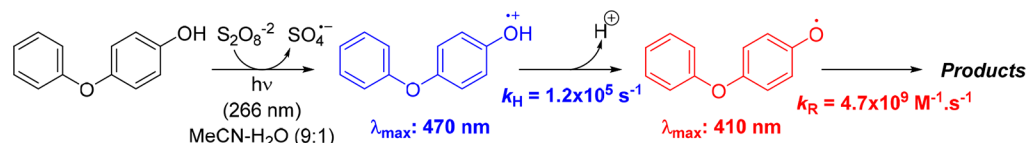
Scheme 1. Direct Irradiation (266 nm) of *Para*-Substituted Phenols in Homogeneous Media^a^aPhenol radical cation and phenoxyl radical transients.

Figure 1. Time-resolved transient absorption spectra recorded with a laser pulse (200 μ s; 266 nm) of acetonitrile solutions (5.1×10^{-4} M) of (a) *p*-tert-butylphenol; (b) *p*-methoxyphenol; (c) *p*-chlorophenol; and (d) *p*-cyanophenol.

Scheme 2. Direct Irradiation (266 nm) of *p*-Phenoxyphenol in an Acetonitrile/Water (9:1) Mixture in the Presence of $K_2S_2O_8$ ($0.010 \text{ mol}\cdot\text{dm}^{-3}$)

phenoxyphenol radical-cation with a maximum wavelength located at 470 nm. Then, the signal located at a maximum wavelength of 405 nm was assigned to the *p*-phenoxyphenoxyl radical which was formed by deprotonation of the radical cation. These experiments clearly show that both transients, the radical-cation and the radical, are formed immediately after the laser pulse and that the radical-cation subsequently loses a proton to provide the radical in the 10 μ s time scale. Additionally, the transient decay traces of a solution of *p*-phenoxyphenol in acetonitrile in the presence of sodium persulfate were recorded at 410 and 460 nm, respectively (see Figure 2b). The decay trace at 460 nm shows a biexponential decay trace yielding two

lifetime values: τ_H 8.1 μ s and τ_R 26.4 μ s, respectively. This behavior can be interpreted considering that both transient species, the phenol radical-cation and the phenoxyl radical, react through consecutive and different pathways, viz. release of a proton from the phenol radical-cation and chemical reaction of the phenoxyl radical (see Scheme 2) as it was observed in earlier reported data.^{9,16} The deprotonation process of the phenol radical-cation is a unimolecular pathway, and the rate constant (k_H) of this process can be calculated from the reciprocal of the lifetime, $k_H = 1/\tau_H$. The value of the rate constant k_H of the *p*-phenoxyphenol radical-cation was found to be $1.2 \times 10^5 \text{ s}^{-1}$. Similar behavior was observed when the transient decay trace

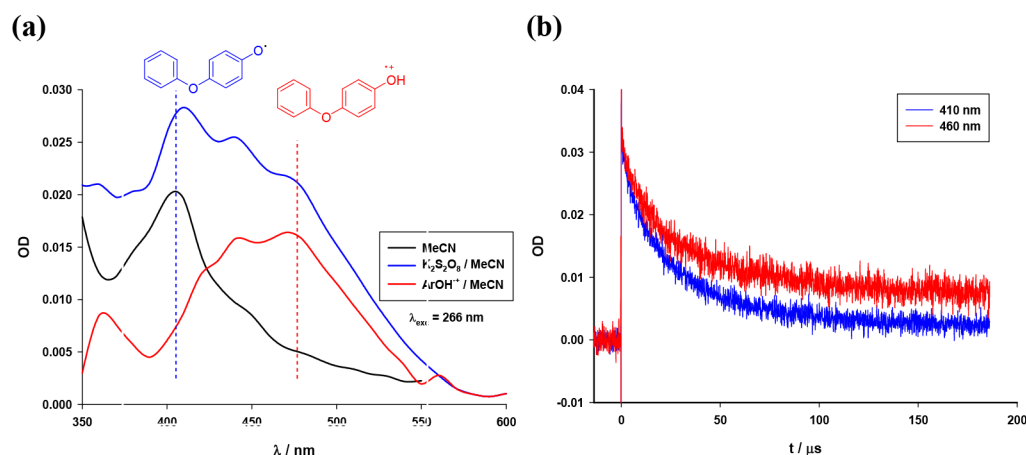


Figure 2. (a) Transient absorption spectra obtained at zero time after the laser pulse ($200 \mu\text{s}$; 266 nm) of solutions ($5.1 \times 10^{-4} \text{ M}$) of p -phenoxyphenol in acetonitrile (black line) and in acetonitrile in the presence of sodium persulfate (blue line) under nitrogen atmosphere and the differential spectrum of the p -phenoxyphenol radical cation (red line). (b) Transient decay traces recorded at 410 and 460 nm after the laser pulse (λ_{exc} : 266 nm) of a solution ($5.1 \times 10^{-4} \text{ M}$) of p -phenoxyphenol in acetonitrile in the presence of sodium persulfate under N_2 atmosphere.

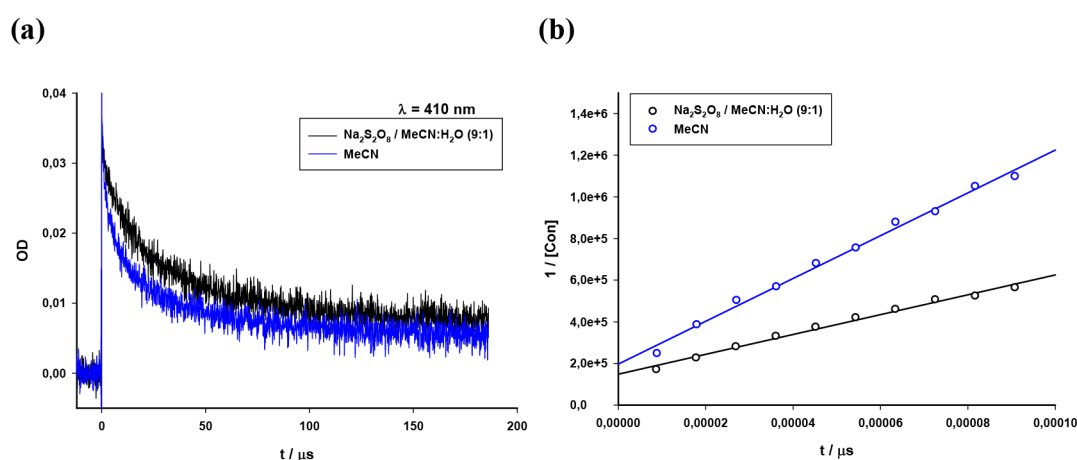


Figure 3. (a) Transient decay traces recorded at 410 nm after the laser pulse ($200 \mu\text{s}$; λ_{exc} : 266 nm) of solutions ($5.1 \times 10^{-4} \text{ M}$) of p -phenoxyphenol in acetonitrile in the absence (blue solid line) and in the presence of sodium persulfate (black solid line) under N_2 atmosphere and room temperature. (b) Reciprocal plotting ($1/\text{concentration}$) vs time in acetonitrile in the absence (blue circles) and in the presence of sodium persulfate (black circles). In all the linear fitting regressions: $R^2 > 0.99$.

Table 1. Spectroscopic Data of Transients from 4-Substituted Phenol Measured by Laser Flash Photolysis (266 nm) in different Solvents under N_2 Atmosphere^a

R	cyclohexane			acetonitrile			methanol		
	λ_{abs} (nm)	τ_{H} (μs)	τ_{R} (μs)	λ_{abs} (nm)	τ_{H} (μs)	τ_{R} (μs)	λ_{abs} (nm)	τ_{H} (μs)	τ_{R} (μs)
OMe	405	4.6	16.0	405	5.0	29.6	405	7.9	38.2
OPh	400	1.3	20.0	405	4.3	38.1	405	6.3	38.2
Me	405	4.4	25.9	405	5.8	41.4	405	4.7	39.1
<i>t</i> -Bu	410	3.8	22.3	410	1.6	19.1	400	5.2	30.7
H	400	4.7	22.2	400	6.2	42.2	400	5.0	23.0
Ph		insoluble		340	0.6	42.4	340	0.2	66.3
Cl	400	2.8	19.6	410	1.9	22.2	410	1.9	14.0
CN	435	1.0	12.2	435	0.7	15.8	435	0.7	24.6
NO_2		insoluble		400	0.8	34.9	400	1.0	58.2

^aConcentration of 4-substituted phenols: $5.0 \times 10^{-4} \text{ M}$. Errors: ± 0.2 .

was analyzed at 410 nm. A biexponential fitting of the transient decay trace was observed (see Figure 2(b); blue solid line) and a rate constant k_{H} of $1.3 \times 10^5 \text{ s}^{-1}$ was obtained from the reciprocal of the short lifetime (τ_{H}). Therefore, the rate constants k_{H} obtained from the analyses of the transient decay

traces at 460 nm and at 410 nm, respectively, were found to be similar values within the experimental error.

The transient decay trace of p -phenoxyphenoxy radical in acetonitrile (solid blue line in Figure 3a) and in a mixture of acetonitrile and water (9:1) in the presence of sodium persulfate

Table 2. Deprotonation (k_H) and Reaction (k_R) Rate Constants of 4-Substituted Phenoxy Radicals and 4-Substituted Phenoxy Radical-Cation Measured by Laser Flash Photolysis (266 nm) in Different Solvents under N_2 Atmosphere^a

R	acetonitrile		methanol		cyclohexane		pK_a^b
	k_H (s^{-1})	k_R ($M^{-1} s^{-1}$)	k_H (s^{-1})	k_R ($M^{-1} s^{-1}$)	k_H (s^{-1})	k_R ($M^{-1} s^{-1}$)	
OMe	2.0×10^5	2.1×10^{10}	1.3×10^5	2.1×10^{10}	2.2×10^5	5.4×10^{10}	4.7
OPh	2.3×10^5	1.0×10^{10}	2.1×10^5	5.0×10^9	7.7×10^5	9.8×10^9	
Me	1.7×10^5	2.2×10^{10}	1.6×10^5	2.8×10^{10}	2.3×10^5	5.3×10^{10}	7.1
<i>t</i> -Bu	6.3×10^5	7.4×10^9	1.9×10^5	1.0×10^{10}	2.6×10^5	2.4×10^{10}	7.2
H	1.6×10^5	5.1×10^9	2.0×10^5	7.6×10^9	2.1×10^5	1.5×10^{10}	8.1
Ph	1.6×10^6	1.9×10^9	5.0×10^6	2.0×10^9	insoluble		5.7
Cl	5.3×10^5	2.3×10^{10}	5.3×10^5	7.1×10^9	3.6×10^5	3.6×10^{10}	9.9
CN	1.5×10^6	2.9×10^{10}	1.4×10^6	3.2×10^{10}	1.0×10^6	3.9×10^{10}	13.0
NO_2	1.6×10^5	1.7×10^{10}	1.0×10^6	1.6×10^{10}	insoluble		15.0

^aConcentration of 4-substituted phenols: 5.0×10^{-4} M. Errors: $\pm 10\%$. ^bData taken from ref 11c.

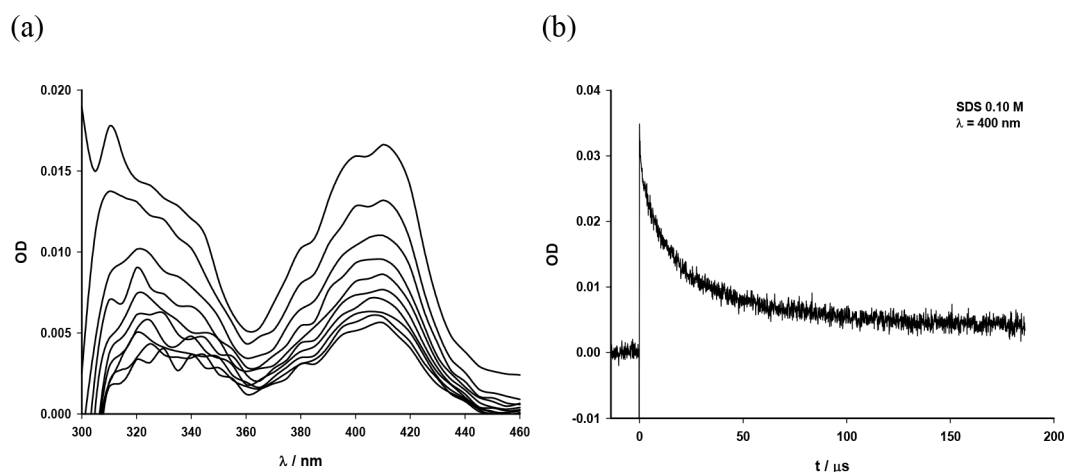


Figure 4. (a) Time-resolved transient absorption spectra recorded with a laser pulse (200 μs ; 266 nm) of *p*-methoxyphenol (5.1×10^{-4} M) in SDS 0.10 M aqueous solutions. (b) Transient decay trace recorded at 400 nm after the laser pulse (λ_{exc} : 266 nm) of *p*-methoxyphenol (5.1×10^{-4} M) in SDS 0.10 M aqueous solutions under N_2 atmosphere.

(solid black line in Figure 3a) was measured at 410 nm showing clearly a biexponential behavior. The bimolecular rate constants (k_R) were determined by plotting the reciprocal of the concentration of the radical transient against time and excellent linear correlations were observed (see Figure 3b). Then after applying a linear regression fitting, the reaction rate constants (k_R) were obtained from the slopes. The second-order rate constant (k_R) was found to be $4.7 \times 10^9 M^{-1} \cdot s^{-1}$ in acetonitrile water (9:1) mixture in the presence of sodium persulfate, while in neat acetonitrile a value of $1.0 \times 10^{10} M^{-1} \cdot s^{-1}$ was obtained. It is noteworthy that the bimolecular rate constants (k_R) measured in both media are slightly different. We could attribute these results to the difference in polarity and proticity of the solvents used; it seems reasonable to propose that *p*-phenoxyphenyloxy radical could diffuse differently within the bulk of both reaction solvents.

The same data analysis was applied to the transient absorption spectra of the remaining *para*-substituted derivatives (Chart 1), recorded in polar and nonpolar solvents such acetonitrile, methanol, and cyclohexane (see Figure S1 in the Supporting Information). The transient decay traces at the maximum absorption wavelength were measured (see Figure S2 in the Supporting Information) showing a biexponential behavior. The spectroscopic data thus obtained are collected in Table 1. The absorption wavelength do not change significantly from nonpolar to polar solvents while it is apparent that the

deprotonation lifetime (τ_H) values of the phenol radical-cation depend on the nature of the substituents. In fact, electron-donor substituents attached to the phenol moiety impose higher lifetime values than the one registered for those phenols bearing electron-withdrawing substituents.

Deprotonation rate constants (k_H) and reaction rate constants (k_R) are reported in Table 2. All of the *para*-substituted phenols in cyclohexane, acetonitrile, and methanol show excellent fitting with the kinetic model proposed (see Figure S3 in the Supporting Information). The slopes obtained after application of linear regression fittings to those straight lines provided k_R values of 10^9 – $10^{10} M^{-1} \cdot s^{-1}$ (Table 2).

It is apparent from Table 2 that the bimolecular rate constants k_R do not show any substituent effect on the reactivity of the phenoxy radicals because the values are under diffusion control in each solvent, and we can suggest that as quickly as the reactants (phenoxy radical or solvent molecules) encounter each other they react. However, the deprotonation rate constants (k_H) do depend on the nature of the substituents. As can be seen in Table 2, the deprotonation rate constant values change from $1.6 \times 10^5 s^{-1}$ to $5.7 \times 10^6 s^{-1}$ as the substituents move from electron-donating to electron-withdrawing ones.

Irradiation of *Para*-Substituted Phenols in Micellar Solution with a Laser Pulse. Direct irradiation of a series of *para*-substituted phenols (for structures, see Chart 1) in aqueous SDS (0.10 M) was carried out with a 266 nm laser

under nitrogen atmosphere, and also in this case, both the phenol radical-cation and the phenoxy radical were formed after the laser pulse. The time-resolved transient absorption spectra of *p*-methoxyphenol in SDS 0.10 M aqueous solutions is depicted as an example in Figure 4a. Its transient radical-cation showed a broad absorption band located between 390 and 490 nm, while the *p*-methoxyphenoxy radical showed two characteristic bands centered at 320 nm and 400–410 nm, values similar to those reported in the literature^{9,15} as well as to those recorded in homogeneous media (see Figure S1 in the Supporting Information). Furthermore, the spectroscopic feature in terms of shape and band location for *p*-methoxyphenol transients in micellar solution are also observed and found similar to those time-resolved absorption spectra recorded for the other *para*-substituted phenol in micellar solution (see Figure S1 in the Supporting Information).

Figure 4b depicts a transient decay trace recorded at 400 nm after the laser pulse (λ_{exc} 266 nm) of *p*-methoxyphenol in SDS 0.10 M aqueous solution under N_2 atmosphere showing a biexponential behavior. After fitting, the short lifetime τ_{H} (lower than 10 μs) was assigned to the *para*-substituted phenol radical-cations while the phenoxy radicals are those species showing lifetimes higher than 20 μs (τ_{R}). The lifetime (τ_{H} and τ_{R}) and the absorption wavelength (λ_{abs}) of the band associate to the lower energy transitions are collected in Table 3. It is apparent from

Table 3. Spectroscopic, Lifetime, and Deprotonation (k_{H}) and Reaction (k_{R}) Rate Constants of 4-Substituted Phenoxy Radicals and 4-Substituted Phenoxy Radical-Cation Measured by Laser Flash Photolysis (266 nm) in Microheterogeneous Media (SDS 0.10 M) under N_2 Atmosphere^a

R	λ_{abs} (nm)	τ_{H} (μs)	τ_{R} (μs)	k_{H} (s^{-1})	k_{R} ($\text{M}^{-1} \text{s}^{-1}$)
OMe	435	9.1	47.2	1.1×10^5	7.0×10^9
OPh	452	1.6	50.9	6.3×10^5	2.6×10^9
Me	425	4.6	34.6	2.2×10^5	1.2×10^{10}
<i>t</i> -Bu	428	4.4	31.6	2.3×10^5	6.3×10^9
H	425	1.8	20.9	5.6×10^5	7.7×10^8
Ph	395	21.3	141.5	4.7×10^4	7.7×10^8
Cl	433	3.6	45.3	2.8×10^5	1.4×10^9
CN	460	9.1	75.0	1.1×10^6	2.2×10^{10}
NO_2	450	0.2		5.6×10^6	

^aConcentration of *para*-substituted phenols: 5.0×10^{-4} M. Errors: ± 0.2 in lifetime values and $\pm 10\%$ in rate constants.

these data that the deprotonation lifetime (τ_{H}) values of the phenol radical-cations depend on the nature of the substituents. In fact, electron-donor substituents attached to the phenol moiety show lifetime values higher than those phenols bearing electron-withdrawing substituents. Otherwise, no clear substituent effect was observed for the τ_{R} values or for the absorption wavelengths (λ_{abs}).

As already described, the deprotonation rate constants (k_{H}) of the *para*-substituted phenol radical-cations were easily calculated from the reciprocal of the short lifetime values ($k_{\text{H}} = 1/\tau_{\text{H}}$) and are also shown in Table 3. On the other hand, plotting the reciprocal of the concentration of the *para*-substituted phenoxy radicals versus time provided an excellent linear fit (see Figure S3 in Supporting Information). Then the reaction rate constants (k_{R}) for all the *para*-substituted phenols were obtained from the slopes after application of linear regression fittings to those straight lines. The k_{R} values of 10^9 – $10^{10} \text{ M}^{-1} \cdot \text{s}^{-1}$ are also collected in Table 3.

As for the homogeneous solutions, it is apparent from the table that no clear substituent effect is observed in SDS micellar solution for the bimolecular rate constants k_{R} , in contrast to k_{H} . Indeed, the k_{H} values change from $1.1 \times 10^5 \text{ s}^{-1}$ to $5.6 \times 10^6 \text{ s}^{-1}$ as the substituents move from electron-donor to electron-withdrawing ones. This effect was quantified plotting $\log(k_{\text{H}}^{\text{R}}/k_{\text{H}}^{\text{R=H}})$ versus the σ^+ Hammett parameters²² (see Figure S5 in the Supporting Information), and after linear regression fittings of the straight line a ρ value of 1.01 was obtained. This value indicated that electron-withdrawing substituents accelerate the deprotonation reaction of the *para*-substituted phenols, and the substituent effect was transmitted efficiently like in substituted benzoic acids.

Quantification of the Substituent and Solvent Effects.

The substituent effect was quantified employing the linear Hammett correlation and the best linear correlation fittings were obtained when σ^+ Hammett parameters were used (see Figure 4a). The Hammett linear free-energy relationship (LFER) is described by eq 2

$$\log(k_{\text{H}}(\text{R}))/\log(k_{\text{H}}(\text{H})) = \rho \cdot \sigma^+ \quad (2)$$

where $k_{\text{H}}(\text{R})$ is the deprotonation rate constant of *para*-substituted phenol radical-cations, $k_{\text{H}}(\text{H})$ is the deprotonation rate constant of unsubstituted phenol radical-cation, ρ is the slope of the linear regression and σ^+ are the Hammett substituent constants.²² Figure 5a shows a linear correlation between the $[\log(k_{\text{H}}^{\text{R}})/\log(k_{\text{H}}^{\text{R=H}})]$ and the substituent constant (σ^+) providing a ρ value of 0.61 ($R^2 > 0.90$). This positive value indicates that the deprotonation rate constants (k_{H}) are sensitive to the electronic effects of the substituents attached to the aromatic ring. Thus, electron-donating groups cause a decrease of the deprotonation rate constants due to a noticeable stabilization of the phenol radical-cation by resonance effect while electron-withdrawing groups cause an increase of the rate constants. However, the sensitivity observed in *para*-substituted phenols is lower than what is observed in *para*-substituted benzoic acids: the ρ value < 1 indicates a lower transmission of the substituent effect.

The radical-cation deprotonation process (see Scheme 1) accounts for the acidity of such transients and appears to parallel, quite regularly, the thermodynamic acidity. Indeed, the plot of the deprotonation rate constants k_{H} as $\text{p}k_{\text{H}}$ vs $\text{p}K_{\text{a}}^{11\text{c}}$ of the *para*-substituted phenol radical-cations (Brønsted plot) is satisfactorily linear (see Figure 5(b)). The Brønsted coefficient α values are quite similar for the two sets of reaction solvents used, *viz.* $\alpha = 0.10$ in MeCN and MeOH, while $\alpha = 0.13$ in cyclohexane and SDS 0.10 M. The similarity of the α values demonstrates the reliability of the $\text{p}K_{\text{a}}$'s reported in Table 2.²³ In our experiments, we suggest that the possible bases for the deprotonation to occur could be the residual H_2O for the experiments carried out in MeCN and MeOH, while in cyclohexane or micellar solution (SDS) the bases are the *para*-substituted phenols themselves. Finally, we can also suggest that the base does not play a significant role in the transition-state structure due to the similar Brønsted coefficients exhibited by such structurally different bases as H_2O and *para*-substituted phenols.

Finally, we have studied the solvent effect on the deprotonation pathway of the *para*-substituted phenol radical-cations using the $E_{\text{T}}(30)$ Reichardt's solvent polarity parameter,²⁴ while the $E_{\text{T}}(30)$ parameter for a micellar solution of SDS in water was calculated from the E_{T}^{N} solvent parameter reported in the literature.²⁵ Figure 6 came of plotting $\log(k_{\text{H}})$ values of some *para*-substituted phenols bearing electron-donor and

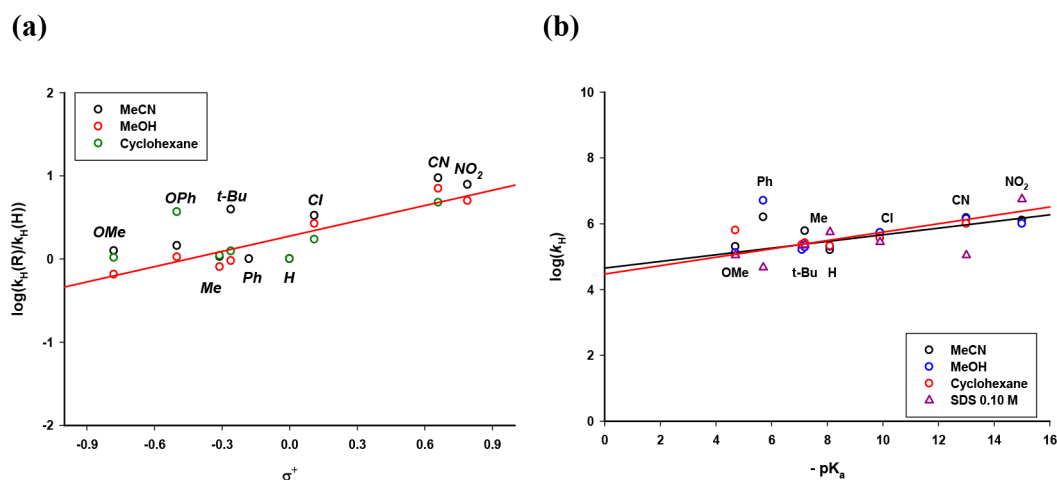


Figure 5. (a) Linear Hammett correlation of deprotonation rate constants (k_H) of *para*-substituted phenol radical-cations versus σ^+ in homogeneous media. (b) Brønsted linear correlation between acid constant (pK_a) and deprotonation rate constants (pK_H) of *para*-substituted phenol radical-cations in homogeneous and micro-heterogeneous media. Best linear fitting in MeCN and MeOH is represented by the black line while the best linear fitting in cyclohexane and SDS 0.1 M is represented by the red line.

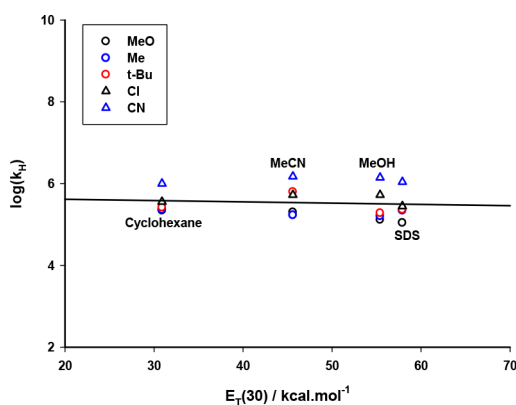


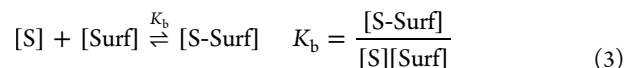
Figure 6. Correlation of the $\log(k_H)$ of *para*-substituted phenol radical-cations against the $E_T(30)$ solvent polarity parameter.

electron-withdrawing substituents against the solvent $E_T(30)$ values but no linear correlation was observed.

This behavior indicates that the solvent is not involved in the deprotonation pathway of the radical-cations because, for each *para*-substituted phenol, the k_H values are similar in nonpolar, polar aprotic, and polar protic solvents as well as in the hydrophobic core of SDS micelle. However, as it was previously pointed out in the text, the phenol radical-cation deprotonation process depends on the acidity of such transients and correlates satisfactorily with the pK_a values according to the Brønsted plots (see Figure 5b), providing lower Brønsted coefficient α values in two sets of solvents, viz. $\alpha = 0.10$ in MeCN and MeOH while $\alpha = 0.13$ in cyclohexane and SDS 0.10 M.

Binding Constants (K_b) of *Para*-Substituted Phenols in Micellar Media. Micellar solutions, which are often considered as micro-photochemical reactors, are micro-heterogeneous systems where photoreactions can be performed. In this regard, we have conducted UV-vis and 2D ¹H NMR spectroscopy studies of *para*-substituted phenols in micellar solution in order to know the positioning of the reactant within the micelles. Thus, we have determined the binding constant (K_b) between the SDS micelles and *para*-substituted phenols employing UV-vis spectroscopy applying a methodology that has been previously reported for aryl acetamide and aryl benzoates.²⁶

Then, the binding of the *para*-substituted phenols to the SDS surfactant that took place within the hydrophobic core of the micelle was demonstrated, analyzing the bathochromic and hyperchromic shifts of the lower energy absorption band of the phenols in water by addition of increasing amounts of surfactant. Indeed, the binding of the *para*-substituted phenols to the micelle can be described according to eq 3 where K_b is the binding constant, S represents the phenols, Surf the surfactants, and [S-Surf] the complex formed between phenols and the surfactant.



Application of Lambert–Beer law on eq 3 provided eq 4 where A_0 and A are the absorbances at the maximum wavelength in the absence and presence of surfactant, respectively, ϵ_C is the molar absorptivity of the complex, and ϵ_S is the *para*-substituted phenols molar absorptivity. Rearranging eq 4 gave eq 5 where a linear relationship is observed between $[A_0/(A - A_0)]$ and the reciprocal of the concentration of the surfactant.

$$\frac{(A - A_0)}{A_0} = \frac{\epsilon_C K_b [\text{Surf}]}{\epsilon_S (1 + K_b [\text{Surf}])} \quad (4)$$

$$\frac{(A - A_0)}{A_0} = \frac{\epsilon_S}{\epsilon_C} + \frac{\epsilon_S}{\epsilon_C K_b} \frac{1}{[\text{Surf}]} \quad (5)$$

Figure 7 shows the data obtained for some *para*-substituted phenols and SDS, including the best linear regression curves, while the straight lines and the corresponding linear regression curves for the other *para*-substituted phenols are collected in Figure S6 (see the Supporting Information). The K_b values for the *para*-substituted phenols were calculated from the ratio of the slope and the intercept of the regression curve (Table 4). Likewise, the calculation of the error of the binding constant K_b values were determined from the intercept, slope and their corresponding error values according to the mathematical method clearly described in the Supporting Information (data shown in Table S1). The K_b values obtained for the *para*-substituted phenols are typical of aromatic solutes as pointed out by Quina, Treiner, and co-workers,²⁷ and estimation of K_b values

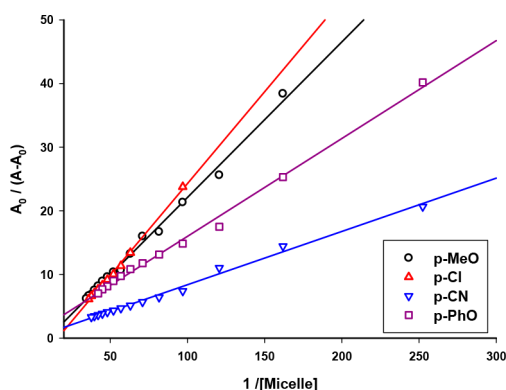


Figure 7. Plot of the $A_0/(A - A_0)$ values of some selected *para*-substituted phenols vs the reciprocal concentration of the micelle in SDS (0.10 M).

$\leq 100 \text{ M}^{-1}$ in SDS for weakly hydrophobic substrates have also been reported.²⁸ Likewise, similar K_b values have been reported for the binding of anionic, cationic, and neutral surfactants and a series of benzoyl chloride derivatives, aryl acetanilides, and aryl benzoates, respectively.^{26,29}

Once the binding constants of the *para*-substituted phenols have been measured, the next step was to confirm qualitatively the location of the phenols within the hydrophobic core of the micelle employing 2D NMR spectroscopy. Determination of the extent of coaggregation in water between two different kinds of surfactants as well as the localization of substrates inside the micelle NOESY experiments have been often used.^{26,30} Satisfactory results are obtained from NOESY experiments when cross-peaks between diagnostic signals of the substrate and the surfactants, respectively, are noticed in the corresponding contour plots.²⁶ Thus, Figure 8 shows the NOESY experiment performed in D_2O for a solution of SDS (100 mM) in the presence of *p*-cyano phenol (7 mM) at room temperature and in the same figure the labels of the protons of the surfactant SDS and the *p*-cyano phenol are also depicted. The inset red frames recognize the NOE (Nuclear Overhauser Effect) between the signals belonging to the aromatic protons (H-2/H-6 and H-3/H-5) of *p*-cyano phenol and the signals of the surfactant SDS such as α , β , ω , and the bulk protons. Similar spectroscopic results have been obtained for solutions of SDS in D_2O in the presence of *p*-methoxy phenol (see Figure S7 in the Supporting Information). The cross-peaks of diagnostic signals observed in the 2D NMR contour plots are in agreement with and reinforce the UV-vis spectroscopic analyses. However, we cannot estimate precisely the location of the phenols with accuracy but we can suggest that the *para*-substituted phenols are located within the hydrophobic core of the micelle because the proton nuclei of the phenols correlate nicely with the proton nuclei of the surfactant as can be seen through the cross-peaks of the contour plots.

TD-DFT Calculations for Prediction of UV-vis Absorption Spectra of *Para*-Substituted Phenol Radical-Cations and Radicals.

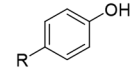
The results of TD-DFT calculations for the UV-vis absorption spectra of *para*-substituted phenol radical-cations and radicals, respectively, in terms of predicted maximum absorption wavelength values but reported as energy values (ΔE) have been collected in Table 5 together with those experimental ΔE values obtained from the transient absorption spectra recorded after the laser pulse (266 nm). The TD-DFT simulation was carried out using Gaussian 16 (Revision B.01 software package),³¹ and the geometry of the molecules was optimized and the thermochemistry was obtained using the (U) ω B97XD/def2SVP level of theory. The UV-vis spectra were simulated at the SMD-(U) ω B97XD/def2TZVP level (solvent: vacuum, cyclohexane, and acetonitrile), computing the lowest 25 singlet transitions and the UV-vis band was plotted as ϵ vs λ (excitation wavelength in nm) with the peaks, furnished by the calculation, assuming a Gaussian band shape (characterized by a standard deviation $\sigma = 0.4 \text{ eV}$) and using the equation for the simulated spectra according to the one described in the Gaussian White Papers.³² All the predicted UV-vis absorption spectra of *para*-substituted phenol radical-cations are collected in Figure S8 (see the Supporting Information) while those belonging to the *para*-substituted phenoxyl radicals are shown in Figure S9 (see the Supporting Information).

Next, we attempted to build a correlation between the theoretical $\Delta E_{(\text{theo})}$ values and the experimental ones ($\Delta E_{(\text{exp})}$), the corresponding plots being shown in Figure 9. Fairly good linear correlations have been obtained for all the *para*-substituted phenol transients excluding the *p*-nitrophenol radical-cation as well as the *p*-nitro- and *p*-phenylphenoxy radical in each linear regressions (see the corresponding arrows in Figure 9).

The linear correlations between the predicted and experimental lower absorption band of *para*-substituted phenol radical-cation and *para*-substituted phenoxyl radicals have been obtained with slopes close to unity and acceptable *R*-square values (see Table 6).

These results demonstrate that the prediction of the $\Delta E_{(\text{theo})}$ using the adopted theoretical approach is fairly accurate leading to a good estimation of the energies values. However, these results deserve some comments. As for *para*-substituted phenol radical-cations (Figure 9a), their energy values span a quite wide range, viz. from 2.73 to 3.24 eV, and the points seem to distribute quite uniformly across the whole range. An exception is constituted by compound 9 showing an important deviation from the linear regression (see the data points indicated with an arrow in Figure 9a). The observed deviation of the data points of compound 9 can be attributed to the theoretical prediction of a nonplanarity of the nitro group with respect to the aromatic plane and thus, canceling the expected bathochromic shift of the absorption band that the theoretical data should correctly be

Table 4. Constants of Binding (K_b) of the *Para*-Substituted Phenols Measured in Micro-heterogeneous Media (SDS 0.10 M)^a

	OMe	OPh	t-Bu	Me	H	Ph	Cl	CN	NO ₂
K_b / M^{-1}	20.13 ±1.39	4.03 ±2.35	19.61 ±2.32	37.20 ±12.11	15.79 ±1.64	6.92 ±1.53	15.79 ±1.64	14.14 ±5.02	7.92 ±0.14

^aErrors: calculations described in the Supporting Information.

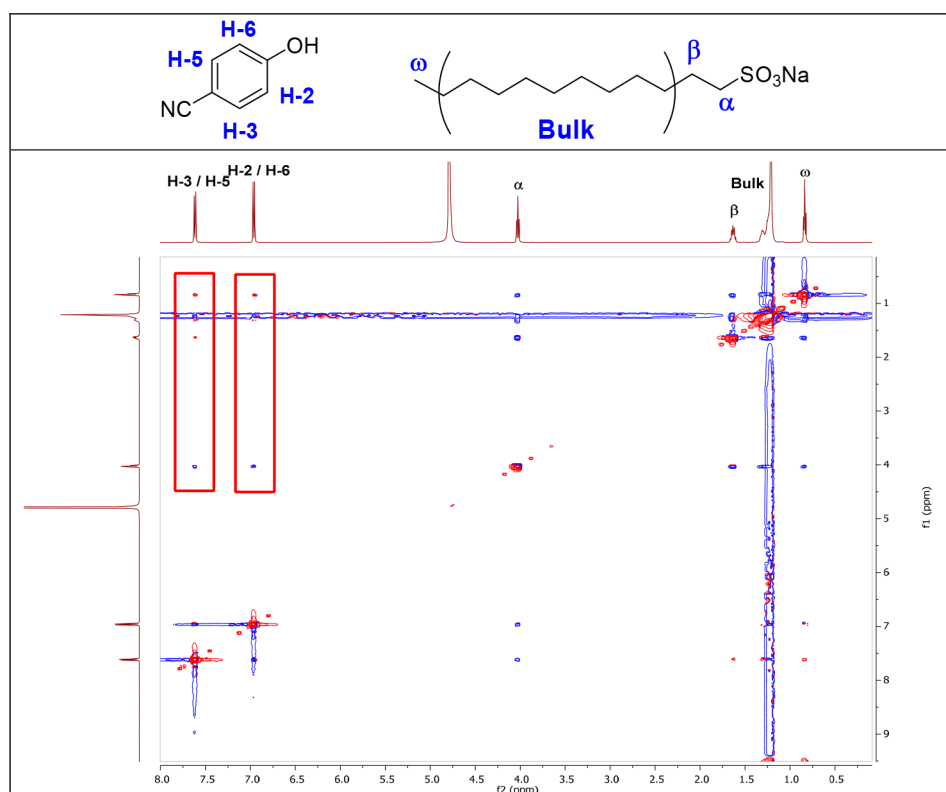
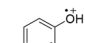
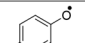


Figure 8. 2D NOESY contour plot of a solution of SDS (100 mM) and *p*-cyanophenol (7 mM) in D₂O at room temperature was recorded with a 500 MHz spectrometer.

Table 5. Experimental and DFT Calculation of the Lower Absorption Band Energies (ΔE) of the *Para*-Substituted Phenol Radical-Cations and *Para*-Substituted Phenol Radicals Measured in Different Solvents

	$\Delta E / \text{eV}^a$ (experimental values)				$\Delta E / \text{eV}^b$ (theoretical values)	
	MeCN	MeOH	Cyclohexane	SDS	MeCN	Cyclohexane
OMe	2.81	2.81	2.84	2.84	3.20	3.17
OPh	2.75	2.75	2.73	2.72	3.21	3.21
Me	2.93	2.89	2.91	2.87	3.31	3.28
t-Bu	2.83	2.87	2.89	2.86	3.26	3.21
H	2.86	2.86	2.91	2.88	3.40	3.38
Ph	3.24	3.21	Insoluble	3.12	3.70	3.60
Cl	2.84	2.87	2.85	2.84	3.07	2.99
CN	2.72	2.69	2.69	2.69	2.97	2.81
NO ₂	2.84	2.81	Insoluble	2.83	3.71	3.75

	$\Delta E / \text{eV}^a$ (experimental values)				$\Delta E / \text{eV}^b$ (theoretical values)	
	MeCN	MeOH	Cyclohexane	SDS	MeCN	Cyclohexane
OMe	3.00	3.04	3.12	3.00	3.70	3.65
OPh	3.04	3.02	3.04	3.04	3.46	3.46
Me	3.05	3.04	3.06	3.03	3.59	3.58
t-Bu	3.04	3.04	3.05	3.08	3.59	3.58
H	3.08	3.08	3.08	3.48	3.71	3.69
Ph	3.59	3.52	Insoluble	3.04	3.43	3.43
Cl	2.90	3.07	3.08	3.13	3.49	3.45
CN	2.83	2.81	2.81	2.83	3.38	3.33
NO ₂	3.08	3.16	Insoluble	3.05	4.40	4.40

^aMeasured by laser flash photolysis (266 nm) under N₂ atmosphere. Concentration of *para*-substituted phenols: 5.0×10^{-4} M. Errors: ± 0.02 . ^bValues calculated with SMD-(U) ω B97XD/def2TZVP level (solvent: cyclohexane and acetonitrile).

predicted. Indeed, the theoretical values that were calculated in acetonitrile and cyclohexane, respectively, have predicted a hypsochromic shift of the lower absorption band which is not the spectroscopic shift observed experimentally. Moving to the

para-substituted phenoxyl radicals (Figure 9b) a fairly linear correlation was also obtained between the theoretical and experimental energy values with exclusion of the data belonging to *p*-nitro- and *p*-phenylphenoxyl radicals which are indicated with black arrows in Figure 9b. This anomalous behavior can be again ascribed to the peculiar nonplanar arrangement of the nitro and phenyl groups with respect to the aromatic plane.

DISCUSSION

The results presented in this paper report for the first time the absolute rate constants for the deprotonation pathway (k_H) of *para*-substituted phenol radical-cations and the reaction pathway (k_R) of *para*-substituted phenoxyl radicals in different solvents such as homogeneous solvents (cyclohexane, acetonitrile, and methanol) and SDS micellar solution (Tables 2 and 3). These data were obtained from the nonlinear regression analyses of the transient decay traces showing biexponential decay behavior (Figure S2 in the Supporting Information). Indeed, the observed transient decay behavior is attributed to the formation of two transient species, viz. the phenol radical-cation and the phenoxyl radical, after direct irradiation of a series of *para*-substituted phenols with a laser pulse of 266 nm in different solvents and micellar solution. Furthermore, we were able to characterize both transient species in terms of lifetime values (Tables 1 and 3) showing shorter lifetime values (lower than 10 μ s) in the case of *para*-substituted phenol radical-cations, while larger ones (higher than 20 μ s) were obtained for *para*-substituted phenoxyl radicals. Likewise, the time-resolved absorption spectra of the *para*-substituted phenols were also measured in homogeneous solvents and SDS micellar solution (Figure 1 and Figure S1 in the Supporting Information) and resulted to be the overlapping of the absorption spectra of the

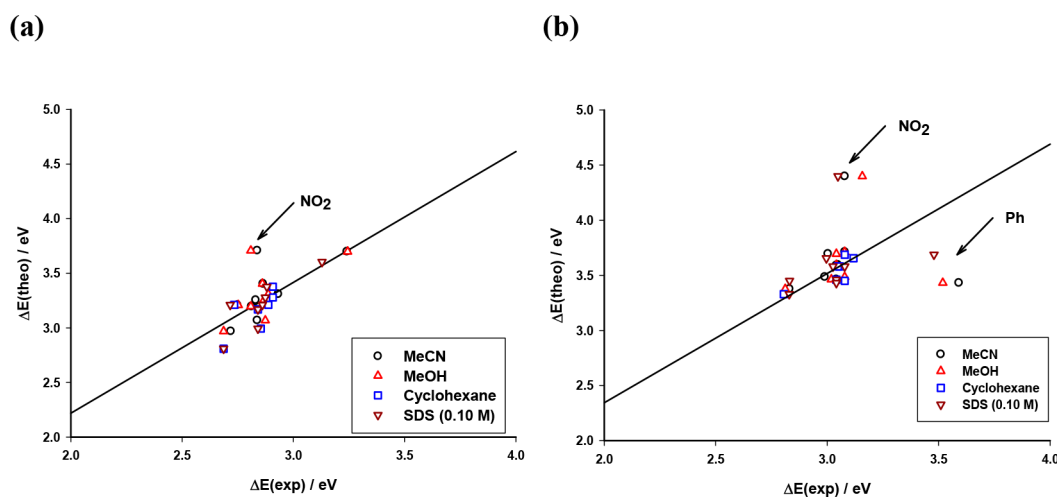


Figure 9. Correlation of the theoretical and experimental energies of the lower absorption band of: (a) *para*-substituted phenol radical-cation and (b) *para*-substituted phenoxyl radicals.

Table 6. Linear Correlation between Experimental and DFT Calculations of the Lower Absorption Band Energies (ΔE) of the *Para*-Substituted Phenol Radical-Cations and *Para*-Substituted Phenol Radicals

transient	$\Delta E_{(\text{theo})} = a\Delta E_{(\text{exp})} + b$		
	<i>a</i>	<i>b</i>	<i>R</i> ²
<i>para</i> -substituted phenol radical-cations	1.20	−0.18	0.79
<i>para</i> -substituted phenoxyl radicals	1.17	0.00	0.95

transient radical-cations with those of the absorption spectra of the corresponding *para*-substituted phenoxyl radicals. The spectra we have obtained agree well with those available in the literature after making allowance for slight solvent-induced shifts.^{9,15}

The effect of the substitution on the absorption maxima of the phenol radical-cations and the phenoxyl radicals but calculated as energy values (ΔE) is interesting (Table 5). While a bathochromic shift of the absorption maximum is observed for all the substituents studied, a notable blue shift is observed for the case of the phenyl group. Even though a trend in the energy values moving to shorter values is noticed with increasing Hammett σ_p values, no well-defined relationship was found. The peculiar behavior of the phenyl group was observed in transients, the radical-cation as well as the phenoxyl radical and can be attributed to the nonplanarity of the phenyl group with respect to the plane of the aromatic ring. Furthermore, this spectroscopic behavior was observed in different solvents (cyclohexane, acetonitrile, and methanol) and also in SDS micellar solution.

The Hammett linear correlation of deprotonation rate constants (k_H) of the *para*-substituted phenol radical-cations leads to $\rho = 0.61$ (Figure 5a) when the data were obtained in cyclohexane, acetonitrile and methanol, whereas in SDS micellar solution the ρ value was 1.01 (Figure S5 in the Supporting Information). Both values are higher in magnitude than that obtained for some *para*-substituted phenols in *n*-butyl chloride ($\rho = 0.31$).³³ This behavior can be attributed to the different polarity and proticity of the solvents used in our study, including the hydrophobic core of the SDS micellar solution. The deprotonation behavior of the phenol radical-cations is explained by electronic effects of the substituents. Indeed, the positive ρ value implies that electron-donating groups such as

methoxy, phenoxy, methyl, and *tert*-butyl groups stabilize the radical-cations causing less spin density at the oxygen of the phenol.

Conversely, electron-withdrawing groups (chloro, ketone, cyano, and nitro) pull electrons away from the aromatic ring destabilizing the corresponding radical-cations and leading to higher spin density at the oxygen of the phenol. Furthermore, the positive ρ values obtained in our experiments account for the nucleophilic character of the *para*-substituted phenol radical-cations during the deprotonation process. By contrast, the substituent effect on the k_R rate constants was also attempted, but no linear relationship was observed because the rate constants are almost diffusion-controlled rates, which render the process insensitive to substituent effects.

On the other hand, it was observed that the rate constants of deprotonation process (k_H) of the *para*-substituted phenol radical-cations correlate nicely with the thermodynamic acidity (pK_a) leading to satisfactory Brønsted plots (Figure 5(b)). The Brønsted coefficient thus obtained ($\alpha = 0.10$ in MeCN and MeOH and $\alpha = 0.13$ in cyclohexane and SDS 0.10 M) clearly indicates a transition-state structure very close to that of the reactants with a very small degree of O–H bond cleavage, as expected for exergonic reactions.²³ Interestingly, smaller Brønsted coefficients have been reported for the case of deprotonation of polymethylbenzene radical-cations and α -substituted *p*-methoxytoluene coming to the same conclusion regarding the corresponding transition-state.^{23b,c}

Two possible bases could be involved during the deprotonation process of the radical-cations, *viz.* H₂O or the *para*-substituted phenols, depending on the reaction solvent used during the irradiations. Thus, we suggest that residual water is the base present during the experiments carried out in MeCN and MeOH while irradiations carried out in cyclohexane and SDS micellar solution the bases are the respective *para*-substituted phenols. In the former case, the substituted phenols cannot be ruled out as possible bases together with water. However, we have concluded that the base does not play a significant role in the transition-state structure due to the similar Brønsted coefficients exhibited by such structurally different bases as H₂O and *para*-substituted phenols. As far as we know, these are the first examples of Brønsted plots for the deprotonation of *para*-substituted phenol radical-cations.

We have demonstrated that micellar solutions are effective micro reactors where photochemical reaction of phenols can occur. Indeed, the irradiation with a laser pulse of 266 nm of *para*-substituted phenols provided transients radical-cations and phenoxy radicals as it was observed in homogeneous media. The photochemical reaction of phenols in SDS micellar solution does involve the deprotonation pathway of the radical-cations and the consecutive reactivity of the phenoxy radicals as can be judged from the data collected in Table 3 and Figure S1 (Supporting Information) in terms of lifetime, rate constants (k_H and k_R) and time-resolved UV–vis absorption spectra of the respective transients. Therefore, these spectroscopic data in micellar media were successfully measured because *para*-substituted phenols were solubilized within the hydrophobic core of the micelle, a confined environment, where the phenols were able to absorb light of 266 nm, photoionized and provide the corresponding radical-cations and the phenoxy radicals within the micelle. Spectroscopic measurements were carried out to confirm the binding of phenols to the micelle and their location within the hydrophobic core. Indeed, UV–vis spectroscopy was used to measure the binding constant (K_b) of *para*-substituted phenols with SDS surfactant according to eq 4 and the values thus obtained (Table 4) tell us that are typical values for aromatic solutes as it was reported in the literature.^{26–29} Furthermore, estimation of K_b values $\leq 100 \text{ M}^{-1}$ in anionic, cationic and neutral surfactants have been previously reported pointing out that the binding of the phenols with the surfactant, in our case surfactant SDS, proceeded efficiently. Likewise, cross peaks of the 2D NMR spectra (Figure 8) clearly show that a nice correlation exists between the aromatic protons (H-2/H-6 and H-3/H-5) of *p*-cyanophenol with all the characteristic protons of the surfactant (α , β , bulk and ω protons) meaning that the aromatic protons are in close contact with any portion of the aliphatic chains of the surfactant. Therefore, we suggest that the disorder in the arrangement of the aliphatic chains within the hydrophobic core of the micelle is responsible for the NOE (Nuclear Overhauser effect) between the aromatic protons and all the surfactant protons. The contour of the 2D NMR spectra led to recognize that after efficient binding of the phenols to the micelle, the phenols locate qualitatively within the micelle core. The location of the phenols cannot be established with accuracy because of the limitation of the 2D NMR methodology.

Finally, we were able to predict the UV–vis absorption spectra of *para*-substituted phenol radical-cations and radicals, respectively, by using TD-DFT calculations (Figures S8 and S9 in the Supporting Information), and then the predicted maximum absorption wavelength values reported as energy values ($\Delta E_{(\text{theo})}$) have been correlated with those experimental $\Delta E_{(\text{exp})}$ values obtained from the transient absorption spectra recorded after the laser pulse (266 nm). Fairly good linear correlations have been obtained with slopes closer to unity reflecting that the prediction of the $\Delta E_{(\text{theo})}$ using the adopted theoretical approach leads to a good estimation of the energies values. However, *p*-nitro- and *p*-phenylphenols deviate from the linear regression, and we suggested that this behavior can be attributed to the fact that both substituents are clearly twisted respect to the plane of the aromatic ring when the analyses were carried out on the transients radical-cation and the corresponding phenoxy radical. Furthermore, the twisting of the substituents entails to a hypsochromic shift of the maximum absorption wavelengths, canceling the bathochromic shift expected experimentally. Noteworthy, a reasonably good linear correlations was observed for the experimental values ($\Delta E_{(\text{exp})}$)

obtained in all the solvents we have studied (cyclohexane, acetonitrile, methanol, and SDS micellar solution).

CONCLUSIONS

The photochemical behavior of a series of *para*-substituted phenols under laser flash photolysis with a pulse of 266 nm has been examined in this paper and two transients; viz. phenol radical-cations and phenoxy radicals are formed after the laser pulse in homogeneous and micellar media. These intermediates were characterized in terms of UV–vis absorption spectra, lifetimes (τ_H and τ_R) and rate constants (k_H and k_R).

The substituent effect was analyzed according to Hammett correlations, and good linear regressions were obtained when $\log(k_H)$ was plotted versus the substituent parameters σ^+ whereas k_R rate constants do not show any Hammett correlation because are almost diffusion-controlled rates which render the process insensitive to substituent effects. The substituent effect on the deprotonation rate constants k_H effectively demonstrated that electron-withdrawing substituents increase the acidity of the phenoxy radical-cations generating the corresponding phenol radicals whereas electron-donor substituents operate oppositely. Furthermore, the deprotonation rate constants k_H was also found to correlate nicely with the $\text{p}K_a$ values in the Brønsted plots of the *para*-substituted phenol radical-cations. The Brønsted coefficients α values thus obtained from the slopes clearly indicated a transition-state structure very close to that of the reactants with a very small degree of O–H bond cleavage. This experimental evidence on the early transition-state structure is reported for the first time demonstrating that the acidity of the phenoxy radical-cations are not so stronger as would be expected.

The photochemical reaction of the *para*-substituted phenols proceeded efficiently also in micellar solution, and the phenol radical-cations, as well as the phenoxy radicals, were formed within the hydrophobic core of the micelle after the laser pulse of 266 nm and were spectroscopically characterized. We have demonstrated that the phenols bind to the micelle measuring the corresponding binding constants (K_b) by using UV–vis spectroscopy. Location of the *para*-substituted phenols within the shell or the hydrophobic core of the micelle was achieved employing 2D NOESY NMR spectroscopy. Therefore, these results have demonstrated that the photochemical reaction takes place efficiently within the micelle, which behaves like a photochemical microreactor. On the other hand, the substituent effect on the deprotonation rate constants k_H measured in a confined hydrophobic environment showed a similar substituent effect as it was observed in homogeneous media demonstrating once again that electron-withdrawing substituents increases the acidity of the phenoxy radical-cations also in micellar media. Furthermore, Brønsted plots obtained for the phenol radical-cations in SDS solution also evidenced the proposal of an early transition-state structure because the Brønsted coefficient α value measured in micellar solution is similar to that obtained in cyclohexane.

Finally, TD-DFT calculations led to predict the energy ($\Delta E_{(\text{theo})}$) values associated with the maximum absorption wavelengths of the transients and were correlated with the energy values ($\Delta E_{(\text{exp})}$) experimentally obtained. Fairly good linear regressions have been obtained with slopes close to unity, reflecting that the prediction of the $\Delta E_{(\text{theo})}$ using the adopted theoretical approach leads to a reasonable estimation of the energies values.

Our study provides evidence for the efficient formation of *para*-substituted phenol radical-cations after the laser pulse that collapses into the corresponding phenoxyl radicals. The deprotonation rate constants of the radical-cations depend on the nature of the substituents and correlate well with the pK_a . A systematic study on the photochemical behavior of the *para*-substituted phenols was carried out for the first time and we hope that the spectroscopic data presented in this paper will be useful for the readership in the understanding the photochemistry of phenols.

EXPERIMENTAL SECTION

Materials and Equipment. *Para*-substituted phenols, potassium persulfate, and sodium dodecyl sulfonate were obtained from commercial sources. Spectroscopic grade solvents were used as received. 2D NOESY spectra were recorded in D_2O on a 500 MHz spectrometer, using a NOESY-ph pulse sequence with a 600 ms mixing time and a recovery delay of 1.5 s. 2K data points were collected for 512 increments of 16 scans, using TPPI f1 quadrature detection; chemical shifts (δ) are reported in part per million (ppm), relative to the signal of trimethylsilylpropionic acid, used as internal standard. The measurements were carried out using standard pulse sequences. Structural assignments were made with additional information from COSY, HSQC, and HMBC experiments. The UV–vis spectra were measured with a Shimadzu UV-1203 spectrophotometer using two-faced stoppered quartz cuvettes (1 mm \times 1 mm) at 298 K.

Determination of the Binding Constants (K_b) of *Para*-substituted Phenols in Micellar Media. Solutions of *para*-substituted phenols were prepared in deionized water (Milli-Q), and their concentrations varied between 5.5×10^{-5} M and 1.0×10^{-4} M. An aliquot (2 mL) of the *para*-substituted phenol solution was placed in a fluorescence-stoppered quartz cuvette provided with a stirring bar, and the UV–vis spectrum was recorded. The initial absorbance value at the maximum absorption wavelength (A_0) was read. Subsequently, aliquots (10 μ L) of concentrated surfactant solution (0.10 M) were added. The UV–vis spectra were registered, recording for each solution the A value at the maximum absorption wavelength. After each addition of surfactant, the solution was stirred for 20 min before measuring the absorbance. With the values of A_0 and A in hand, the values of ($A_0/(A - A_0)$) versus the reciprocal of the concentration of the micellar surfactant were plotted, and the data were fitted with a linear regression program. The K_b values were obtained by calculating the ratio of the slope and the origin.

Laser Flash Photolysis. The laser pulse photolysis apparatus consisted of a Flash lamp-pumped Q-switched SpitLight-100 Nd:YAG laser from InnoLas used at the fourth harmonic of its fundamental wavelength. The LP920-K monitor system (supplied by Edinburgh Instruments), arranged in a cross-beam configuration, consisted of a high-intensity 450 W ozone free Xe arc lamp (operating in pulsed wave), a Czerny–Turner with triple grating turret monochromator, and a five-stage dynode photomultiplier. The signals were captured by means of a Tektronix TDS 3012C digital phosphor oscilloscope, and the data were processed with the L900 software supplied by Edinburgh Instruments. The solutions to be analyzed were placed in a fluorescence cuvette ($d = 10$ mm).

TD-DFT Calculations. The TD-DFT simulation was carried out using Gaussian 16, Revision B.01 software package.³¹ The geometry of the molecules was optimized and the thermochemistry was obtained at the (U) ω B97XD/def2-SVP level of theory. The UV/vis spectra were simulated at the SMD-(U) ω B97XD/def2-TZVP level (solvent: vacuum, cyclohexane, and acetonitrile), computing the lowest 25 singlet transitions.

The UV/vis band was plotted as ϵ vs λ (excitation wavelength in nm) with the peaks, furnished by the calculation, assuming a Gaussian band shape (characterized by a standard deviation $\sigma = 0.4$ eV). The equation for the simulated spectra follows the one described in the Gaussian White Papers³²

$$\epsilon(\lambda) = \sum_{i=1}^n \epsilon_i(\lambda) = \sum_{i=1}^n \left\{ 1.3062974 \times 10^8 \frac{f_i}{10^7} \exp \left[- \left(\frac{1/\lambda - 1/\lambda_i}{\frac{1}{3099.6}} \right)^2 \right] \right\} \quad (1a)$$

with f_i the computed oscillator strengths, referred to a specific wavelength λ_i . For the sake of simplicity, only the information regarding the first five transitions of the species analyzed are reported (see the Supporting Information).

ASSOCIATED CONTENT

Supporting Information

The Supporting Information is available free of charge at <https://pubs.acs.org/doi/10.1021/acs.joc.0c02031>.

UV–vis absorption spectra under time-resolved spectroscopy; transient decay traces at maximum absorption wavelength (λ_{max}); determination of the rate constants k_H and k_R in homogeneous and heterogeneous media; Bronsted plot; Hammett linear correlation plot in heterogeneous media; determination of the constants of binding K_b ; 2D NOESY NMR spectra in micellar media; TD-DFT calculated UV–vis absorption spectra of *para*-substituted phenol transients (PDF)

AUTHOR INFORMATION

Corresponding Author

Sergio M. Bonesi – Universidad de Buenos Aires. Facultad de Ciencias Exactas y Naturales, Departamento de Química Orgánica, C1428EGA Buenos Aires, Argentina; CONICET – Universidad de Buenos Aires. Centro de Investigaciones en Hidratos de Carbono (CIHIDECAR), C1428EGA Buenos Aires, Argentina; Dipartimento di Chimica, Sezione Chimica Organica, University of Pavia, 27100 Pavia, Italy; orcid.org/0000-0003-0722-339X; Phone: +54-11-45763346; Email: smbonesi@qo.fcen.uba.ar

Authors

Gastón Siano – Universidad de Buenos Aires. Facultad de Ciencias Exactas y Naturales, Departamento de Química Orgánica, C1428EGA Buenos Aires, Argentina; CONICET – Universidad de Buenos Aires. Centro de Investigaciones en Hidratos de Carbono (CIHIDECAR), C1428EGA Buenos Aires, Argentina
Stefano Crespi – Stratingh Institute for Chemistry, University of Groningen, 9747AG Groningen, The Netherlands; orcid.org/0000-0002-0279-4903

Complete contact information is available at: <https://pubs.acs.org/doi/10.1021/acs.joc.0c02031>

Notes

The authors declare no competing financial interest.

ACKNOWLEDGMENTS

Sergio M. Bonesi is a research member of CONICET.

REFERENCES

- (1) *Atmospheric Oxidation and Antioxidants*; Scott, G., Ed.; Elsevier: Amsterdam, 1993; Vol. I, Chapter 4, pp 121–160; Vol. II, Chapter 5, pp 161–224, Chapter 3, pp 141–218, Chapter 4, pp 219–277, Chapter 5, pp 279–326

- (2) Schnabel, W. *Polymer Degradation*; Hanser: Muenchen, 1992.
- (3) Brede, O.; Wojnarovis, L. Kinetics of formation and decay of 4-methyl-2,6-di-*t*-butylphenoxy radicals in cyclohexane solution. *Radiat. Phys. Chem.* **1991**, *37*, 537–548.
- (4) Geto, N.; Solar, S. Radiation induced decomposition of chlorinated phenols in water. *Radiat. Phys. Chem.* **1988**, *31*, 121–130.
- (5) Steenken, S.; Neta, P. One-electron redox potentials of phenols. Hydroxy- and aminophenols and related compounds of biological interest. *J. Phys. Chem.* **1982**, *86*, 3661–3667.
- (6) Brede, O.; Orthner, H.; Hermann, R. Phenol-assisted photolytic and radiolytic radical cation formation of a sterically hindered tertiary amine. *Chem. Phys. Lett.* **1994**, *229*, 571–576.
- (7) Bansal, K. M.; Fessenden, R. W. Pulse radiolysis studies of the oxidation of phenols by SO_4^{2-} and Br_2^- in aqueous solutions. *Radiat. Res.* **1976**, *67*, 1–8.
- (8) Brede, O.; Orthner, H.; Zubarev, V.; Hermann, R. Radical cations of sterically hindered phenols as intermediates in radiation-induced electron transfer processes. *R. J. Phys. Chem.* **1996**, *100*, 7097–7105.
- (9) (a) Gadosy, T. A.; Shukla, D.; Johnston, L. J. Generation, characterization, and deprotonation of phenol radical cations. *J. Phys. Chem. A* **1999**, *103*, 8834–8839. (b) Shukla, D.; Schepp, N. P.; Mathivanan, N.; Johnston, L. J. Generation and spectroscopic and kinetic characterization of methoxy-substituted phenoxy radicals in solution and on paper. *Can. J. Chem.* **1997**, *75*, 1820–1829. (c) O'Shea, K. E.; Cardona, C. Hammett study on the TiO_2 catalyzed photo-oxidation of para-substituted phenols. A kinetic and mechanistic analysis. *J. Org. Chem.* **1994**, *59*, 5005–5009.
- (10) (a) Land, E. J.; Porter, G.; Strachan, E. Primary photochemical processes in aromatic molecules. Part 6. The absorption spectra and acidity constants of phenoxy radicals. *Trans. Faraday Soc.* **1961**, *57*, 1885–1893. (b) Land, E. J.; Porter, G. Primary photochemical processes in aromatic molecules. Part 8. Absorption spectra and acidity constants of aniline radicals. *Trans. Faraday Soc.* **1963**, *59*, 2027–2037. (c) Dobson, G.; Grossweiner, L. I. Flash photolysis of aqueous phenol and cresols. *Trans. Faraday Soc.* **1965**, *61*, 708–714. (d) Yamada, H.; Nakashima, N.; Tsubomura, H. Mechanism of photodissociation of hydroquinone derivatives. *J. Phys. Chem.* **1970**, *74*, 2897–2903. (e) Feitelson, J.; Hayon, E.; Treinin, A. Photoionization of phenols in water. Effects of light intensity, oxygen, pH, and temperature. *J. Am. Chem. Soc.* **1973**, *95*, 1025–1029. (f) Feitelson, J.; Hayon, E. Electron ejection and electron capture by phenolic compounds. *J. Phys. Chem.* **1973**, *77*, 10–15. (g) Bent, D. V.; Hayon, E. Excited state chemistry of aromatic amino acids and related peptides. I. Tyrosine. *J. Am. Chem. Soc.* **1975**, *97*, 2599–2606. (h) Brede, O.; Orthner, H.; Zubarev, V.; Hermann, R. Radical cations of sterically hindered phenols as intermediates in radiation-induced electron transfer processes. *J. Phys. Chem.* **1996**, *100*, 7097–7175. (i) Brede, O.; Hermann, R.; Orthner, H. Charge transfer to a semi-esterified bifunctional phenol. *Radiat. Phys. Chem.* **1996**, *47*, 415–417.
- (11) (a) Yi, M.; Scheiner, S. Proton transfer between phenol and ammonia in ground and excited electronic states. *Chem. Phys. Lett.* **1996**, *262*, 567–572. (b) Dixon, W. T.; Murphy, D. Determination of the acidity constants of some phenol radical cations by means of electron spin resonance. *J. Chem. Soc., Faraday Trans. 2* **1976**, *72*, 1221–1230. (c) Bordwell, F. G.; Cheng, J. P. Substituent effects on the stabilities of phenoxy radicals and the acidities of phenoxy radical cations. *J. Am. Chem. Soc.* **1991**, *113*, 1736–1743.
- (12) Sun, Q.; Tripathi, G. N.; Schuler, R. H. Time-resolved resonance Raman spectroscopy of *p*-aminophenol radical cation in aqueous solution. *J. Phys. Chem.* **1990**, *94*, 6273–6277.
- (13) Steadman, J.; Syage, J. A. Picosecond studies of proton transfer in clusters. 2. Dynamics and energetics of solvated phenol cation. *J. Am. Chem. Soc.* **1991**, *113*, 6786–6795.
- (14) (a) Maruyama, K.; Furuta, H.; Osuka, A. CIDNP study on porphyrin-photosensitized reactions with phenol and quinone: dimerization of 4-methoxyphenol and cross coupling of benzoquinone to porphyrins covalently with phenol group. *Tetrahedron* **1986**, *22*, 6149–6155. (b) Dixon, W. T.; Murphy, D. Determination of acid dissociation constants of some phenol radical cations. *J. Chem. Soc., Faraday Trans. 2* **1978**, *74*, 432–439.
- (15) Ganapathi, M. R.; Hermann, R.; Naumov, S.; Brede, O. Free electron transfer from several phenols to radical cations of non-polar solvents. *Phys. Chem. Chem. Phys.* **2000**, *2*, 4947–4955.
- (16) (a) Choure, S. C.; Bamatraf, M. M. M.; Rao, B. S. M.; Das, R.; Mohan, H.; Mittal, J. P. Hydroxylation of chlorotoluenes and cresols: a pulse radiolysis, Laser flash photolysis, and product analysis studies. *J. Phys. Chem. A* **1997**, *101*, 9837–9845. (b) Alfassi, Z. B.; Schuler, R. H. Reaction of azide radicals with aromatic compounds. Azide as a selective oxidant. *J. Phys. Chem.* **1985**, *89*, 3359–3363.
- (17) (a) Bisby, R. H.; Parker, A. W. Reaction of the α -tocopheroxy radical in micellar solutions studied by nanosecond laser flash photolysis. *FEBS Lett.* **1991**, *290*, 205–208. (b) Parker, A. W.; Bisby, R. H. Time-resolved resonance Raman spectroscopy of α -tocopheroxy radical and related radicals in solvent, micellar and membrane systems. *J. Chem. Soc., Faraday Trans.* **1993**, *89*, 2873–2878. (c) Zhou, B.; Wu, L.-M.; Yang, L.; Liu, Z.-L. Evidence for α -tocopherol regeneration reaction of green tea polyphenols in SDS micelles. *Free Radical Biol. Med.* **2005**, *38*, 78–84.
- (18) (a) Kerzig, Ch.; Henkel, S.; Goetz, M. A new approach to elucidating repair reactions of resveratrol. *Phys. Chem. Chem. Phys.* **2015**, *17*, 13915–13920. (b) Kerzig, Ch.; Hoffmann, M.; Goetz, M. Resveratrol radical repair by vitamin C at the micelle-water interface—unexpected reaction rates explained by ion-dipole interactions. *Chem. - Eur. J.* **2018**, *24*, 3038–3044.
- (19) Kerzig, Ch.; Goetz, M. Photoionization access to cyclodextrin-encapsulated resveratrol phenoxy radicals and their repair by ascorbate across the phase boundary. *Phys. Chem. Chem. Phys.* **2016**, *18*, 20802–20811.
- (20) Dzeba, I.; Pedzinski, T.; Mihalievic, B. Photophysical and photochemical properties of resveratrol. *J. Photochem. Photobiol., A* **2015**, *299*, 118–124.
- (21) Aspee, A.; Aliaga, Ch.; Maretti, L.; Zúñiga-Núñez, D.; Godoy, J.; Pino, E.; Cardenas-Giron, G. I.; Lopez-Aarcon, C.; Scaiano, J. C.; Alarcon, E. I. Reaction Kinetics of phenolic antioxidants towards photo-induced pyranine free radicals in biological models. *J. Phys. Chem. B* **2017**, *121*, 6331–6340.
- (22) (a) Hammett, L. P. Some Relations between Reaction Rates and Equilibrium Constants. *Chem. Rev.* **1935**, *17*, 125–136. (b) Hansch, C.; Leo, A.; Taft, R. W. A survey of Hammett substituent constants and resonance and field parameters. *Chem. Rev.* **1991**, *91*, 165–195.
- (23) (a) Lucarini, M.; Pedrielli, P.; Pedulli, G. F.; Cabiddu, S.; Fattuoni, C. Bond Dissociation Energies of O-H Bonds in Substituted Phenols from Equilibration Studies. *J. Org. Chem.* **1996**, *61*, 9259–9263. (b) Baciocchi, E.; Del Giacco, T.; Elisei, F. Proton-Transfer Reactions of Alkylaromatic Cation Radicals. The Effect of α -Substituents on the Kinetic Acidity of *p*-Methoxytoluene Cation Radicals. *J. Am. Chem. Soc.* **1993**, *115*, 12290–12295. (c) Schlesener, C. J.; Amatore, C.; Kochi, J. K. Rates and Mechanism of Proton Transfer from Transient Carbon Acids. The Acidities of Methylbenzene Cations. *J. Am. Chem. Soc.* **1984**, *106*, 7472–7482.
- (24) Reichardt, Ch.; Welton, Th. In *Solvents and Solvent Effects in Organic Chemistry*; Reichardt, Ch., Welton, Th., Eds.; Wiley-VCH Verlag: Weinheim, 2011; Chapter 7, pp 425–508.
- (25) Fuguet, E.; Rafols, C.; Marti, R. Characterization of the Solvation Properties of Surfactants by Solvatochromic Indicators. *Langmuir* **2003**, *19*, 6685–6692.
- (26) (a) Siano, G.; Crespi, S.; Mella, M.; Bonesi, S. M. Selectivity in the photo-Fries rearrangement of some aryl benzoates in green and sustainable media. Preparative and mechanistic studies. *J. Org. Chem.* **2019**, *84*, 4338–4352. (b) Iguchi, D.; Erra-Balsells, R.; Bonesi, S. M. Photo-Fries rearrangement of aryl acetamides: regioselectivity induced by the aqueous micellar green environment. *Photochem. Photobiol. Sci.* **2016**, *15*, 105–116.
- (27) (a) Sepulveda, L.; Lissi, E.; Quina, F. H. Interactions of Neutral Molecules with Ionic Micelles. *Adv. Colloid Interface Sci.* **1986**, *25*, 1–57. (b) Quina, F. H.; Alonso, E. O. Incorporation of Nonionic Solutes into Aqueous Micelles: A Linear Solvation Free Energy Relationship

Analysis. *J. Phys. Chem.* **1995**, *99*, 11708–11714. (c) Abraham, H.; Chadha, H. S.; Dixon, J. P.; Rafols, C.; Treiner, C. Hydrogen bonding Part 40. Factors that influence the distribution of solutes between water and sodium dodecylsulfate micelles. *J. Chem. Soc., Perkin Trans. 2* **1995**, 887–894. (d) Abraham, H.; Chadha, H. S.; Dixon, J. P.; Rafols, C.; Treiner, C. Hydrogen bonding. Part 41.1 Factors that influence the distribution of solutes between water and hexadecylpyridinium chloride micelles. *J. Chem. Soc., Perkin Trans. 2* **1997**, 19–24.

(28) Brinchi, L.; di Profio, P.; Micheli, F.; Germani, R.; Savelli, G.; Bunton, C. A. Structure of Micellar head-Groups and the Hydrolysis of Phenyl Chlorofomate. The Role of Perchlorate Ion. *Eur. J. Org. Chem.* **2001**, *2001*, 1115–1120.

(29) Campos Rey, P.; Cabaleiro Lago, C.; Hervés, P. Solvolysis of Substituted benzoyl Chlorides in Nonionic and Mixed Micellar Solutions. *J. Phys. Chem. B* **2010**, *114*, 14004–14011.

(30) (a) Sabatino, P.; Szczygiel, A.; Sinnaeve, D.; Hakimhashemi, M.; Saveyn, H.; Martins, J. C.; van der Meeren, P. NMR study of the influence of pH on phenol sorption in cationic CTAB micellar solutions. *Colloids Surf, A* **2010**, *370*, 42–48. (b) Voets, I. K.; de Keizer, A.; de Waard, P.; Frederik, P. M.; Bomans, P. H. H.; Schmalz, H.; Walther, A.; King, S. M.; Leermakers, F. A. M.; Cohen Stuart, M. A. Doubled-faced micelles from water-soluble polymers. *Angew. Chem., Int. Ed.* **2006**, *45*, 6673–6676. (c) Yuan, H. Z.; Zhao, S.; Cheng, G. Z.; Zhang, L.; Miao, X. J.; Mao, S. Z.; Yu, J. Y.; Shen, L. F.; Du, Y. R. Mixed micelles of Triton X-100 and Cetyl triammonium bromide in aqueous solution studied by ¹H NMR. *J. Phys. Chem. B* **2001**, *105*, 4611–4615.

(31) Frisch, M. J.; Trucks, G. W.; Schlegel, H. B.; Scuseria, G. E.; Robb, M. A.; Cheeseman, J. R.; Scalmani, G.; Barone, V.; Petersson, G. A.; Nakatsuji, H.; Li, X.; Caricato, M.; Marenich, A. V.; Bloino, J.; Janesko, B. G.; Gomperts, R.; Mennucci, B.; Hratchian, H. P.; Ortiz, J. V.; Izmaylov, A. F.; Sonnenberg, J. L.; Williams-Young, D.; Ding, F.; Lipparini, F.; Egidi, F.; Goings, J.; Peng, B.; Petrone, A.; Henderson, T.; Ranasinghe, D.; Zakrzewski, V. G.; Gao, J.; Rega, N.; Zheng, G.; Liang, W.; Hada, M.; Ehara, M.; Toyota, K.; Fukuda, R.; Hasegawa, J.; Ishida, M.; Nakajima, T.; Honda, Y.; Kitao, O.; Nakai, H.; Vreven, T.; Throssell, K.; Montgomery, J. A., Jr.; Peralta, J. E.; Ogliaro, F.; Bearpark, M. J.; Heyd, J. J.; Brothers, E. N.; Kudin, K. N.; Staroverov, V. N.; Keith, T. A.; Kobayashi, R.; Normand, J.; Raghavachari, K.; Rendell, A. P.; Burant, J. C.; Iyengar, S. S.; Tomasi, J.; Cossi, M.; Millam, J. M.; Klene, M.; Adamo, C.; Cammi, R.; Ochterski, J. W.; Martin, R. L.; Morokuma, K.; Farkas, O.; Foresman, J. B.; Fox, D. J., Gaussian, Inc., Wallingford CT, 2016.

(32) <http://dev.gaussian.com/uvvisplot/>.

(33) (a) Hermann, R.; Naumov, S.; Mahalaxmi, G. R.; Brede, O. Stability of phenols and thiophenol radical-cations – interpretation by comparative quantum chemical approaches. *Chem. Phys. Lett.* **2000**, *324*, 265–272. (b) Zhang, H.-Y.; Sun, Y. M.; Wang, X. L. Electronic effects on O-H proton dissociation energies of phenolic cation radicals: a DFT study. *J. Org. Chem.* **2002**, *67*, 2709–2712.